

## Integration of statistical modeling and high-content microscopy to systematically investigate cell–substrate interactions

Wen Li Kelly Chen<sup>a</sup>, Morakot Likhitpanichkul<sup>b</sup>, Anthony Ho<sup>a</sup>, Craig A. Simmons<sup>a,b,c,\*</sup>

<sup>a</sup> Institute of Biomaterials and Biomedical Engineering, University of Toronto, 164 College Street, Toronto, Ontario M5S 3G9, Canada

<sup>b</sup> Department of Mechanical and Industrial Engineering, University of Toronto, 5 King's College Road, Toronto, Ontario, M5S 3G8, Canada

<sup>c</sup> Faculty of Dentistry, University of Toronto, 124 Edward Street, Toronto, Ontario, M5G 1G6, Canada

### ARTICLE INFO

#### Article history:

Received 29 September 2009

Accepted 1 December 2009

Available online 6 January 2010

#### Keywords:

Extracellular matrix  
Mesenchymal stem cell  
Substrate stiffness  
Mechanobiology  
High-content screening

### ABSTRACT

Cell–substrate interactions are multifaceted, involving the integration of various physical and biochemical signals. The interactions among these microenvironmental factors cannot be readily elucidated and quantified by conventional experimentation, and necessitate multifactorial strategies. Here we describe an approach that integrates statistical design and analysis of experiments with automated microscopy to systematically investigate the combinatorial effects of substrate-derived stimuli (substrate stiffness and matrix protein concentration) on mesenchymal stem cell (MSC) spreading, proliferation and osteogenic differentiation. C3H10T1/2 cells were grown on type I collagen- or fibronectin-coated polyacrylamide hydrogels with tunable mechanical properties. Experimental conditions, which were defined according to central composite design, consisted of specific permutations of substrate stiffness (3–144 kPa) and adhesion protein concentration (7–520 µg/mL). Spreading area, BrdU incorporation and Runx2 nuclear translocation were quantified using high-content microscopy and modeled as mathematical functions of substrate stiffness and protein concentration. The resulting response surfaces revealed distinct patterns of protein-specific, substrate stiffness-dependent modulation of MSC proliferation and differentiation, demonstrating the advantage of statistical modeling in the detection and description of higher-order cellular responses. In a broader context, this approach can be adapted to study other types of cell–material interactions and can facilitate the efficient screening and optimization of substrate properties for applications involving cell–material interfaces.

© 2009 Elsevier Ltd. All rights reserved.

### 1. Introduction

The ability to predictably control stem cell differentiation to generate clinically-relevant cell types is essential for many regenerative medicine applications. Traditionally, various exogenous factors (e.g., cytokines, extracellular matrix proteins, and biomaterials) have been used to induce stem cell differentiation, but mostly on a trial-and-error basis using one-factor-at-a-time (OFAT) experiments without systematic consideration of different factor interactions. Given the complexity of cellular responses, the integrated effects of multiple stimulatory cues as opposed to their individual actions may be key to understanding and controlling cell behaviour. The investigation of combined effects of multiple stimuli has become increasingly appreciated not only for its potential

adaptation in tissue engineering strategies, but also for its relevance in basic biology as an approach that better recapitulates physiological conditions [1].

All cells in the body, except those in circulation, require anchorage to a solid matrix to remain viable. Cell functions are dictated by microenvironmental cues from the immediate extracellular milieu. The diverse extracellular matrix (ECM) environment, both the physical and biochemical characteristics of different tissues, alludes to the importance of proper cell–ECM interactions in mediating tissue-specific functions. Dysregulation of cell–ECM interaction, manifested in aberrant ECM production and changes in tissue rigidity, has been linked to various pathological developments [2,3]. Given the importance of ECM cues in regulating cell function, there is the opportunity to artificially engineer an extracellular milieu that predictably guides cell function for applications in regenerative medicine.

Mesenchymal stem cells (MSCs), a candidate cell source for tissue engineering applications, are responsive to a number of ECM-derived signals, including extracellular matrix proteins [4,5] and matrix mechanics [6–8]. The latter, in particular, has been

\* Corresponding author. Department of Mechanical and Industrial Engineering, University of Toronto, 5 King's College Road, Toronto, Ontario, M5S 3G8, Canada. Tel.: +1 416 946 0548; fax: +1 416 978 7753.

E-mail address: [simmons@mie.utoronto.ca](mailto:simmons@mie.utoronto.ca) (C.A. Simmons).

recently recognized as a potent modulator for MSC lineage specification. MSCs were directed to *early* neural, myoblast or osteoblast fate on type I collagen-coated substrates with elasticities comparable to those of brain, muscle and pre-calcified bone, respectively [6]. Moreover, substrate stiffness-mediated MSC differentiation appears to be ECM protein coating-dependent, possibly mediated through the interactions with different integrin receptors, suggestive of an interplay between the substrate mechanics and biochemistry [7]. Indeed, many tissues with comparable mechanical properties, such as those of brain, fat and marrow [8], exhibit distinctive phenotypic and functional characteristics; therefore, fine-tuning of additional ECM signals, such as ECM protein type and concentration, may influence how MSC respond to substrate mechanics. However, cellular functions arising from the integration of multiple microenvironmental cues are complex and non-linear in nature, and are difficult to efficiently detect and describe by conventional experimentation.

Here we report an approach that incorporates statistical modeling with automated, high-content microscopy to facilitate the systematic and efficient investigation of substrate mechanics and adhesive characteristics in regulating MSC proliferation and osteogenic differentiation. The quantitative description of MSC activities as functions of substrate properties allows experimenters to better gauge the contributions from different substrate cues and facilitates their optimization for predictive guidance of stem cell fate. This type of systematic biomaterial screening not only furthers fundamental understanding of stem cell–ECM interactions, but also has practical merits in the development of biomaterials and the improvement of cell culture substrates for research and drug screening applications.

## 2. Materials and methods

### 2.1. Polyacrylamide substrate fabrication

Polyacrylamide (PA) was chosen as a model substrate for its mechanical tunability. The PA substrates were fabricated using a protocol adapted from Pelham and Wang [9]. Briefly, substrates were fabricated by sandwiching PA solution between a Surfasil-treated glass coverslip (diam. 12 mm) and an adhesive plastic backing of similar size designed to support PA adhesion. The bottom adhesive disks were cut from a polyester film (GelBond<sup>®</sup> PAG, Lonza, Burlington, ON, Canada) using a 2" diameter hole punch (Online River, New Canaan, CT, USA). Top cover glass slips were immersed in 10% v/v Surfasil<sup>™</sup> silicizing fluid (Pierce, Rockford, IL, USA) in xylene for 1–3 min, followed by rinsing with xylene, and subsequently with methanol. The treated cover slips were dried in the fume hood. PA substrates of various stiffness (3, 11, 22, 50, 144 kPa) were obtained by changing the concentration of acrylamide (3.0–15%) (BioRad, Mississauga, ON, Canada) and bis-acrylamide (0.10–1.2%) in deionized water and 10 mM of HEPES (Sigma, Oakville, ON, Canada). Polymerization was initiated and catalyzed with the addition of 1/200 volume of 10% ammonium persulfate and 1/2000 volume of n,n,n',n'-Tetramethylethylenediamine (BioRad). 50  $\mu$ L of the syringe-filtered (0.2  $\mu$ m) polymerizing solution was pipetted onto a PA adhesive polyester backing and then a Surfasil-treated cover slip was quickly placed on top. After polymerization, the Surfasil-treated cover slips were removed and the gels were placed in a 24-well and activated for protein conjugation, as described previously [10]. Briefly, the gels were placed in 0.5 mm of *N*-sulfo-succinimidyl-6-(4'-azido-2'-nitrophenylamino) hexanoate (sulfo-SANPAH, Pierce) solution in 0.25% dimethyl sulfoxide (Sigma), 50 mM HEPES and deionized water, and exposed to UV light (365 nm) for 10 min. Photoactivation was repeated once with fresh sulfo-SANPAH solution. After thorough rinsing in 50 mM HEPES and PBS, the substrates were sterilized under UV for 20 min. Adhesion protein coatings were applied at least 4 h after gel fabrication once the gels had finished swelling. The gels were incubated with different concentrations (7, 14, 63, 282, or 520  $\mu$ g/mL) of rat tail type I collagen (Becton Dickinson, Mississauga, ON, Canada) in 0.2 N acetic acid or bovine fibronectin (Sigma) in phosphate-buffered saline (PBS) at 4 °C overnight. The collagen- or fibronectin-functionalized gels were rinsed thrice with PBS prior to cell seeding.

### 2.2. Mechanical characterization of PA substrates

The mechanical properties of the PA gels were determined from unconfined compression tests using a Mach-1 mechanical test machine (BioSyntec Canada Inc, Quebec, Canada), equipped with a 150 g load cell. Cylindrical disks of PA gel (5 mm

diameter and approximately 1 mm thickness) were cored from gel slabs using a biopsy punch and allowed to hydrate and swell to equilibrium one day before testing. The gel specimens were placed between a non-porous indenter and a bottom plate within a chamber containing PBS. A 10% static compressive strain was applied with a ramp velocity of 1  $\mu$ m/s, and held constant to allow for stress relaxation until equilibrium was reached. The Young's moduli of the hydrogels were calculated from the ratio of the recorded stress at equilibrium and the applied strain.

### 2.3. Protein conjugation characterization of PA substrates

To ensure independence of protein coating and PA elasticity, gels were incubated with different concentrations of fluorescein isothiocyanate (FITC)-labelled type I collagen (Exalpha Biologicals Inc., Watertown, MA, USA) in 0.1 N acetic acid overnight in the dark (refer to design matrix in Table 1). The functionalized gels were rinsed extensively to remove unbound collagen prior to imaging. Five fields of each of the functionalized substrates were imaged using a fluorescent microscope (Olympus IX-71, Markham, ON, CA) and camera (Retiga, 2000R, QImaging, Surrey, BC, CA). The fluorescence intensities were quantified using ImageJ (NIH) and analyzed statistically as described in Section 2.6.

### 2.4. Cell culture

A mouse-derived embryonic fibroblast cell line (C3H10T1/2) was used as a model for mesenchymal stem cells due to its ability to differentiate to the osteoblast, adipocyte, chondrocyte or myoblast lineages. The use of a homogeneous cell line eliminates concerns that selective adhesion of committed cells in a heterogeneous MSC population rather than active differentiation was responsible for the lineage specification observed under different substrate conditions. Cells at passage 13 were used for all experiments. Growth media containing 89% Eagle's basal media, 10% fetal bovine serum and 1% penicillin/streptomycin were used for all experiments. Cells were seeded at low density (2500 cell/cm<sup>2</sup>) to reduce cell–cell interactions and paracrine effects.

### 2.5. High-content imaging and response characterization

To accurately and efficiently quantify the response of thousands of cells as a function of multiple stimuli, an ArrayScan<sup>™</sup> high-content imaging system (Cellomics, Pittsburgh, PA, USA) was used. This system uses fluorescent labelling, automated microscopy, and built-in image analysis algorithms to collect and analyze information simultaneously from multiple fluorescent channels at the single cell level. The ability to do single cell analyses in situ has several benefits, including the potential to account for population heterogeneity typical of stem cells and to elucidate spatial relationships that are lost with population-based measures.

Here, cells were stained and scanned directly in the well plates to characterize various cellular functions, as described below. Prior to imaging, the samples were inverted in the well plates to minimize the optical distance between the sample and the objective lens. In addition, ApoTome, an optical sectioning tool in Cellomics, was engaged to improve image focus and to reduce background fluorescence.

**Table 1**

Design matrix for the two-factor central composite design.

Experimental condition	Substrate stiffness (coded) <sup>a,c</sup>	Protein concentration (coded) <sup>b</sup>	Young's modulus (kPa)	Protein concentration ( $\mu$ g/mL)
1	−0.46	−1	11.3	14.1
2	0.62	−1	50.3	14.1
3	−0.46	1	11.3	281.8
4	0.62	1	50.3	281.8
5	−1.33	0	3.4	63.1
6	1.38	0	144.5	63.1
7	0.03	−1.414	22.4	7.6
8	0.03	1.414	22.4	520.6
9	0.03	0	22.4	63.1
10	0.03	0	22.4	63.1
11	0.03	0	22.4	63.1
12	0.03	0	22.4	63.1
13	0.03	0	22.4	63.1

<sup>a</sup> Scaling factor for substrate stiffness: Coded values = (log[Young's Modulus] − 1.33)/0.6.

<sup>b</sup> Scaling factor for protein concentration: Coded values = (log[Protein concentration] − 1.8)/0.65.

<sup>c</sup> The coded values for substrate stiffness slightly deviated from a standard central composite design (CCD) design due to constraints on PA fabrication. Such operational constraints are common in practice and can be compensated for automatically by the statistical software during analysis.

### 2.5.1. Cell spreading

To determine cell spreading area, C3H10T1/2 cells were cultured on gels with different combinations of substrate stiffness and ECM protein type and concentrations (refer to design matrix in Table 1), and were fixed at 20 h post-seeding and stained with FITC-labelled phalloidin (Sigma) and propidium iodide (PI; Sigma) or Hoechst 33342 (Invitrogen). The spreading area of single cells was quantified using the Cellomics *Cell Spreading* assay algorithm. Briefly, Channel 1 (XF100 FITC) was used to identify the cell area labelled by phalloidin, and Channel 2 (XF93 TRITC or XF100 Hoechst) identified the cell nuclei. The total number of pixels measured from the phalloidin-labelled region was converted to cell area reported in  $\mu\text{m}^2$ .

### 2.5.2. Cell cycle quantification

Substrate-dependent proliferation capacity of C3H10T1/2 cells was determined by bromodeoxyuridine (BrdU) incorporation. Cells were cultured on type I collagen- or fibronectin-coated PA substrates for three days (refer to design matrix in Table 1). On day three, cells were fed media containing BrdU and incubated for 2 h prior to the termination of the experiment. Then, the cells were washed once with PBS and fixed in 10% neutral-buffered formalin (NBF) overnight at 4 °C. The percentage of BrdU positive cells was determined by indirect immunofluorescent staining. The fixed cells were washed three times with PBS, and they were treated with 2 N hydrochloric acid for 1 h at 37 °C to denature DNA for BrdU antibody binding. After acid denaturation, the cells were neutralized in 0.1 M borate buffer at pH 8.5 (twice) and rinsed twice with PBS with 0.05% Tween 20. To reduce non-specific antibody binding, the cells were incubated with a blocking solution containing 3% bovine serum albumin (BSA) and 0.1% Tween 20 in  $\text{Ca}^{2+}/\text{Mg}^{2+}$ -free PBS at 37 °C for 1 h. Subsequently, the samples were incubated with primary BrdU antibody in the same blocking solution for at 37 °C for 3 h. The samples were washed extensively to remove unbound BrdU antibodies. For secondary immunostaining, the samples were treated with Alexa Fluor 488 goat anti-mouse IgG (Invitrogen, Burlington, ON, Canada) and PI in PBS with 10% goat serum and 0.05% Tween 20 at 37 °C for 1 h in the dark. The samples were then washed extensively with PBS with 0.05% Tween 20 and deionized water prior to imaging. The Cellomics *Target Activation* algorithm was used for image acquisition and analysis. Briefly, Channel 1 (XF93 TRITC) was used to identify the PI-labelled nuclei, and Channel 2 (XF100 GFP) measured the fluorescence emitted from the nuclear region defined by the primary object selected from Channel 1. A minimum of 3000 cells were imaged per sample. The average intensity measurement from Channel 2 was used to obtain a bimodal fluorescence distribution. Microsoft Excel was used to convert the fluorescence measurements into a series of bimodal fluorescence distribution histograms, where the number of cells under first and second peak corresponded to the BrdU negative and positive fraction, respectively.

### 2.5.3. Osteogenic differentiation

The extent of Runx2 translocation, an early osteochondral transcription factor, was used to determine osteogenic differentiation of C3H10T1/2 cells. Since Runx2 regulates different stages of osteogenesis by binding to promoter sequences of bone-specific proteins [11], its nuclear localization indicates Runx2 activation and early osteogenic commitment. The C3H10T1/2 cells were cultured for 4 days on either type I collagen- or fibronectin-functionalized substrates in growth media to determine the effects of substrate stiffness and ECM protein independent of chemical influence (refer to design matrix in Table 1). On day 4, the cells were rinsed once with PBS and fixed in 10% NBF for 30 min. After rinsing thrice with PBS to remove the fixative, the cells were permeabilized with 0.1% Triton-X100 for 5 min and washed twice with PBS. The samples were blocked as described above and incubated with 1:100 dilution of polyclonal rabbit anti-mouse Runx2 antibody (Santa Cruz Biotechnology, CA, USA) overnight at 4 °C. The samples were washed extensively and incubated with Alexa Fluor 568 goat anti-rabbit IgG (Invitrogen) and counter-stained with Hoechst 33 342 in PBS with 10% goat serum and 0.05% Tween 20 for 1 h at room temperature. The samples were washed extensively with PBS with 0.05% Tween 20 and deionized water. The Cellomics *Molecular Translocation* algorithm was used for image acquisition and analysis. Briefly, Channel 1 (XF53 Hoechst) was used to identify Hoechst-labelled nuclei. Channel 2 (XF53 TRITC) was used to measure fluorescence intensity in regions of interest, which included the nuclear region defined by Hoechst staining in Channel 1 and a cytoplasmic ring region defined by a set distance offset from the nuclear region.

## 2.6. Experimental design and statistical analysis

Statistical experimental design and analysis techniques like factorial design and response surface methodology are useful approaches to investigate the individual and interactive effects of multiple input stimuli. In this study, we used a central composite design (CCD) to characterize significant matrix inputs affecting protein coating and MSC function, including spreading, proliferation and osteogenic specification. CCD was chosen for this particular study because of its efficiency in detecting two-factor interactions and quadratic effects with the minimal use of resources (fewer experimental conditions than full factorial designs) [12]. For a two-factor response surface, the output responses ( $Y$ ) were modeled as a function of the independent inputs ( $x_i$ ) in a polynomial function (Eq. (1)),

$Y = K + \beta_1 x_1 + \beta_2 x_2 + \beta_{12} x_1 x_2 + \beta_{11} x_1^2 + \beta_{22} x_2^2$ , where  $K$  corresponds to the averaged response of centre points,  $\beta_i$  the main effect coefficients,  $\beta_{ij}$  second-order interaction coefficients, and  $\beta_{ii}$  the quadratic coefficients.  $x_i$  corresponds to the coded values of the factor levels. The design matrix and coded values are shown in Table 1. Coded variables were used for the statistical analyses because this approach generates more precise parameter estimations [12] and facilitates interpretation by allowing the comparison of  $\beta$  coefficients to determine factor effects independent of units. Experimental runs were randomized to reduce systematic error. Cellular response measurements were logarithmically transformed to stabilize unequal variances. Model parameter estimation was performed using JMP 8 (SAS Institute) by least squares estimation, a common method used in model building [12]. The  $\beta$  coefficients were calculated, and the statistical significance of each parameter was evaluated, with  $P \leq 0.05$  chosen to denote significance. The model was then optimized through an iterative approach using backward elimination in which insignificant factors ( $P > 0.05$ ) were removed from the model, and then the model parameters were recalculated based on the reduced model. The resultant equation containing significant parameters was used to generate response surfaces to facilitate the visualization of factor effects. In some cases, the removal of insignificant regression coefficients caused the lack-of-fit test to become significant. In those instances, the last deleted insignificant parameter was kept to maintain model adequacy. For the proliferation and differentiation experiments, multiple replicates of the design matrix were run to improve precision.

## 3. Experimental results

### 3.1. Substrate characterization

The elastic moduli of PA hydrogels were found to be 3, 11, 22, 50, and 144 kPa by compression testing (Fig. 1). Fluorescent microscopy demonstrated that the distribution of the adhesion protein (in this case FITC-collagen) was globally uniform (data not shown), with randomly distributed local variations, consistent with previous studies [10]. The independence of surface protein presentation (in this case type I collagen) and gel stiffness was validated by statistical design and analysis of experiment (Table 1), in which FITC-collagen conjugation was modeled as a function of substrate properties by fitting data to a second-order polynomial, as described above. The analyses confirmed that protein conjugation was linearly dependent on protein concentration ( $P < 0.001$ ) and independent of substrate stiffness ( $P = 0.169$ ) and stiffness–protein interaction ( $P = 0.06$ ). Further, the absence of a significant negative 2nd-order protein concentration term indicated a lack of protein saturation behaviour.

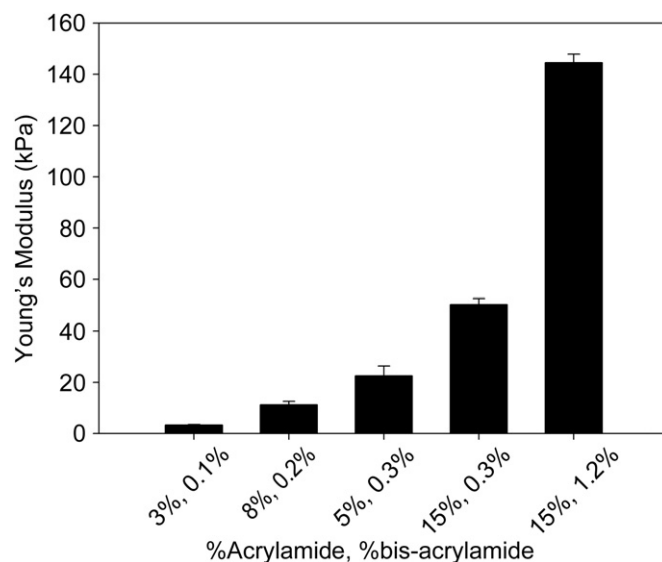


Fig. 1. Mechanical characterization results of PA substrates. The substrate elastic modulus of the PA gels was varied by changing the acrylamide and bis-acrylamide composition.

### 3.2. MSC spreading

As expected, cell spreading area positively correlated with increasing substrate stiffness for both type I collagen- and fibronectin-coated substrates (Fig. 2). Saturation in stiffness-induced spreading was only detected on fibronectin-coated substrates, denoted by the significant quadratic term,  $\beta_{\text{stiffness}^* \text{stiffness}}$  (Figs. 2B and 3B). On collagen-coated substrates, there was less spreading and no saturation stiffness was detected in the experimental range for the time point studied (Figs. 2A and 3A). MSC spreading was independent of collagen or fibronectin concentration, as denoted by the insignificant collagen and fibronectin concentration terms (Fig. 2A and B). Though not statistically significant, a second-order collagen concentration term ( $\beta_{\text{Col I}^* \text{Col I}} = 0.06$ ,  $P = 0.39$ ) was kept in the model (Figs. 2A and 3A) to maintain a non-significant lack-of-fit assumption. Since this  $\beta$  coefficient was close to zero, the contribution of this term to model predictions was negligible.

### 3.3. MSC proliferation

MSC proliferation, determined by the % BrdU incorporation (Supplemental Fig. 1), was modeled as previously described. On collagen-coated substrates, proliferation was stimulated by increasing substrate stiffness ( $\beta_{\text{stiffness}} = 0.15$ ,  $P = 0.01$ ) and inhibited by elevating collagen concentration ( $\beta_{\text{Col I}} = -0.08$ ,  $P = 0.03$ ), as

evidenced by the opposing signs of the respective  $\beta$  coefficients. These effects were independent because the interaction term,  $\beta_{\text{stiffness}^* \text{Col I}}$ , was insignificant ( $P > 0.17$ ). The absolute value of the  $\beta_{\text{stiffness}}$  was approximately two-fold that of the  $\beta_{\text{Col I}}$ , suggesting a dominating effect of substrate mechanics over surface adhesiveness. Proliferation was linearly correlated with substrate stiffness and no saturation was detected in the range of elasticities studied (Fig. 4A), suggestive of a saturating stiffness value at substrate modulus beyond 144 kPa. Though proliferation was inversely correlated with increasing collagen concentration for the whole range of stiffness levels investigated, the parameter estimation was close to zero ( $\beta_{\text{Col I}} = -0.08$ ), indicating a minimal effect on cell expansion.

On fibronectin-coated substrates, MSC proliferation exhibited a prominent biphasic dependence ( $\beta_{\text{stiffness}^* \text{stiffness}} = -0.26$ ,  $P < 0.001$ ;  $\beta_{\text{stiffness}} = -0.31$ ,  $P < 0.0001$ ) on substrate stiffness and was independent of fibronectin concentration (Figs. 2B and 4B). However, the second-order fibronectin term ( $\beta_{\text{Fn}^* \text{Fn}} = 0.035$ ,  $P = 0.62$ ) was required in the model to maintain a non-significant lack-of-fit. Since the absolute value of the  $\beta_{\text{Fn}^* \text{Fn}}$  estimate was only about one tenth of that of  $\beta_{\text{stiffness}^* \text{stiffness}}$ , the incorporation of this non-significant term minimally affected model predictions. By interpolating the response surface (Fig. 4B), a substrate modulus of 9.4 kPa (coded value of  $-0.6$ ) was found to maximize MSC proliferation on fibronectin-coated PA gels on day 3.

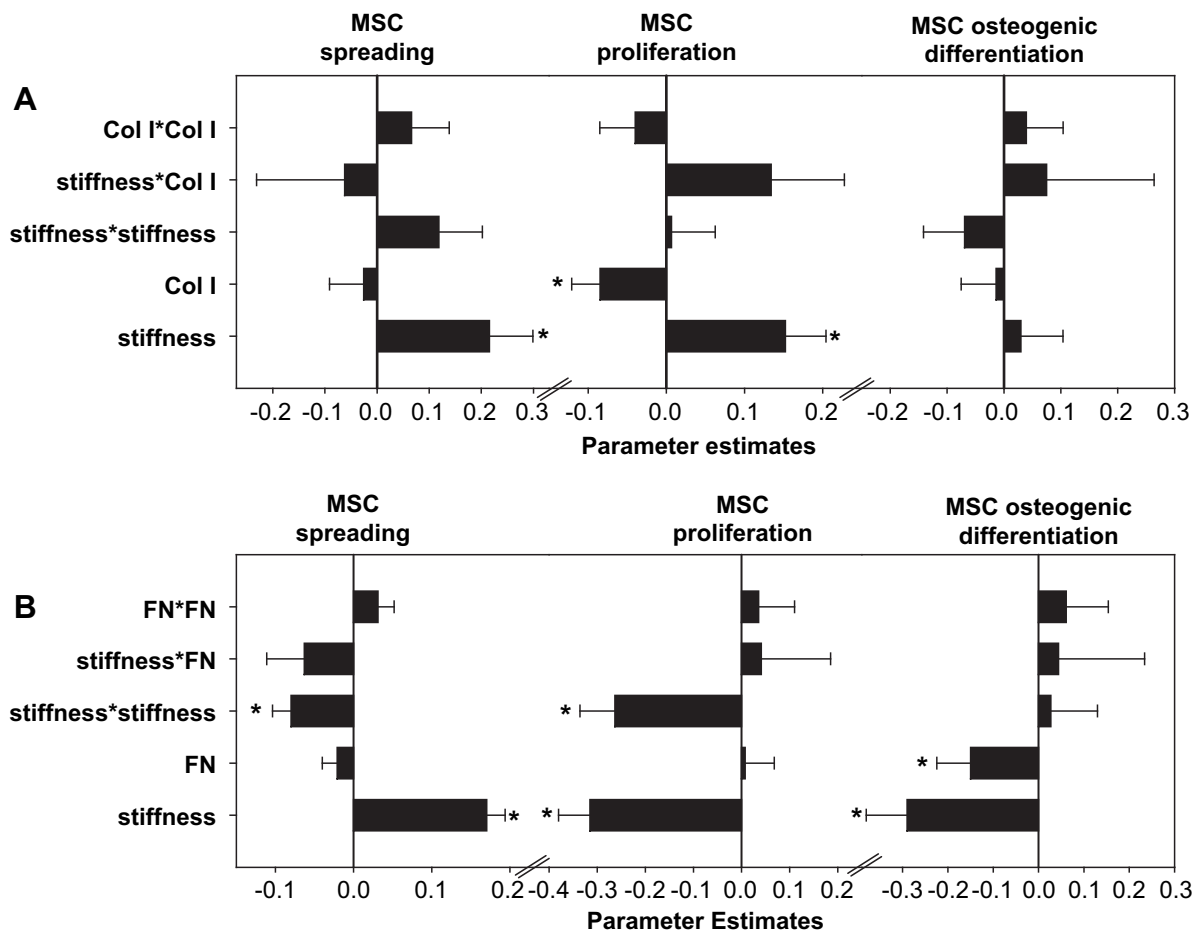


**Fig. 2.** A summary of factor effects (parameter estimations) for MSC activities (i.e., MSC spreading, proliferation or osteogenic differentiation) on (A) Type I collagen- or (B) fibronectin-coated PA substrates. The vertical axis labels correspond to  $\beta$  coefficients in the polynomial function (Eq. (1)) in Section 2.6, where *stiffness* corresponds to  $\beta_1$ , *Col I* or *Fn* corresponds to  $\beta_2$ , *stiffness\*Col I* or *stiffness\*Fn* corresponds to  $\beta_{12}$ , *stiffness\*stiffness* corresponds to  $\beta_{11}$ , and *Col I\*Col I* or *Fn\*Fn* correspond to  $\beta_{22}$ . Error bars represent standard error. \* $P < 0.05$  denotes statistical significance.

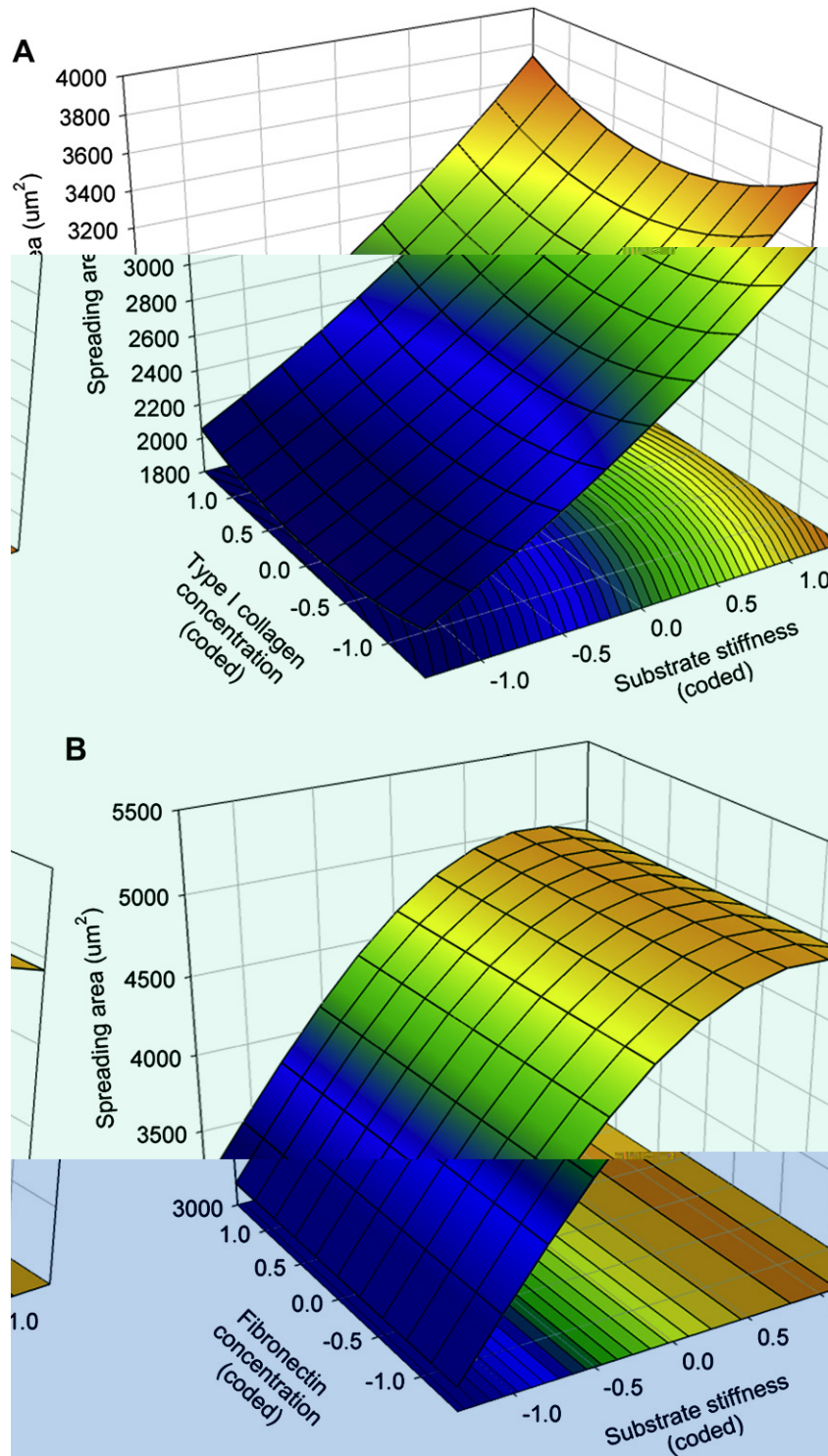


Fig. 3. The response surface of MSC spreading on (A) type I collagen- or (B) fibronectin-coated PA substrates. The definition of the coded values is provided in Table 1.

### 3.4. MSC osteogenic differentiation

The extent of MSC osteogenic differentiation was evaluated by the difference in average Runx2 fluorescent intensity between nuclear and cytoplasmic regions (Supplemental Fig. 2). The response surface for MSCs on collagen (Fig. 5A) revealed there was an interaction between collagen concentration and substrate stiffness, although the model parameters did not reach statistical

significance (Fig. 2A). At low collagen concentration, Runx2 translocation exhibited a biphasic dependence on substrate stiffness with a maximum at 28.4 kPa (coded value of 0.21), while at high collagen concentration, Runx2 translocation revealed a more linear dependence which plateaued only at high stiffness.

On fibronectin-coated substrates, Runx2 nuclear translocation was negatively regulated by substrate stiffness and fibronectin concentration as indicated by the significant  $\beta$  coefficients

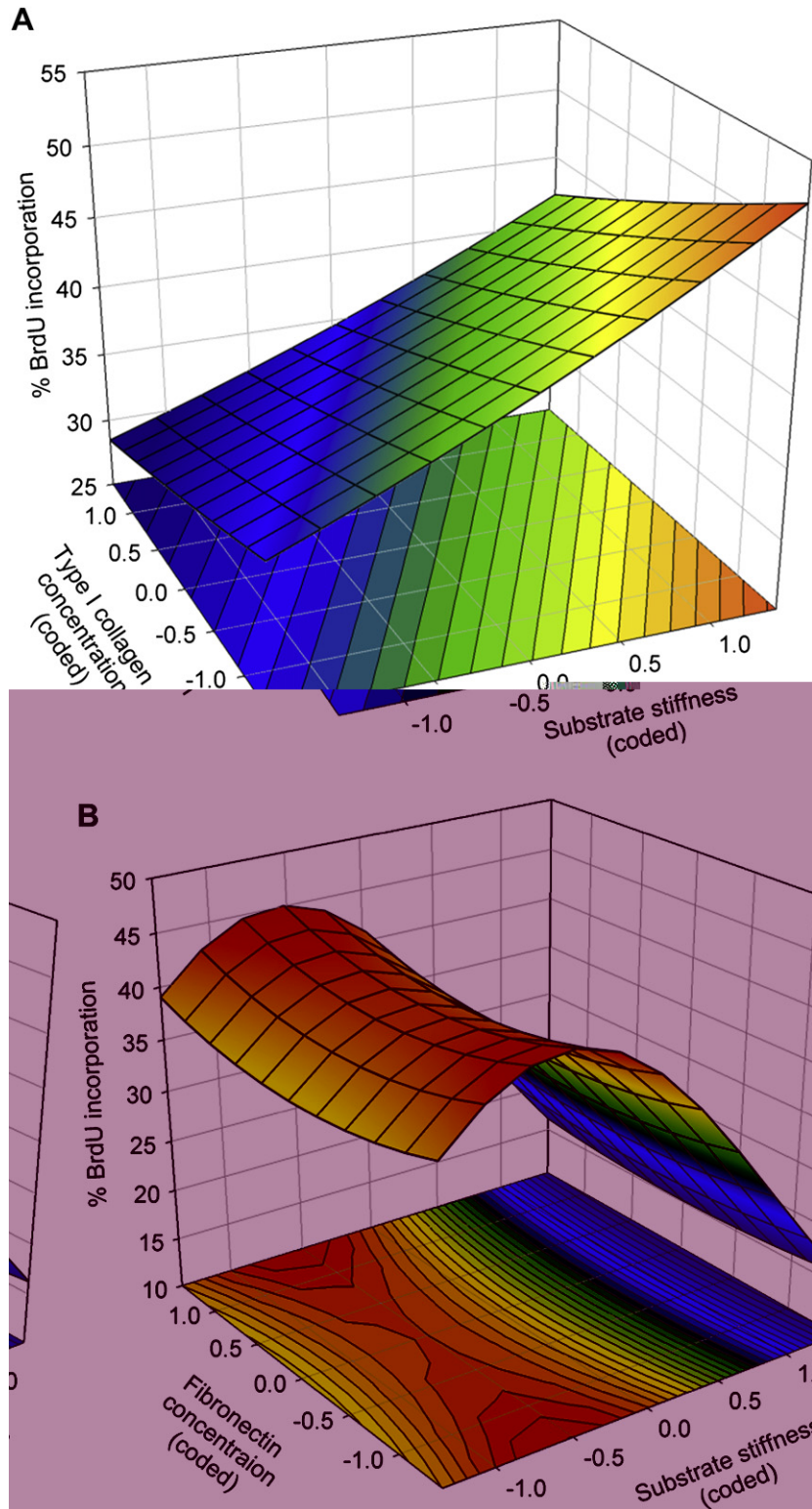


**Fig. 4.** The response surface of MSC proliferation on (A) type I collagen- or (B) fibronectin-coated PA substrates. The definition of the coded values is provided in Table 1.

( $\beta_{\text{stiffness}} = -0.30$ ,  $P = 0.0063$ ;  $\beta_{\text{fibronectin}} = -0.15$ ,  $P = 0.055$ ) (Figs. 2B and 5B). The substrate stiffness effect was twice that of the fibronectin concentration effect, indicating a dominant matrix mechanics influence in regulating Runx2 nuclear translocation. Since the interaction term,  $\beta_{\text{stiffness}^*\text{FN}}$ , was not significant ( $P > 0.85$ ), the negative effects of stiffness and fibronectin concentration were independent and additive.

#### 4. Discussion

Cell–substrate adhesion precedes most biological processes while anchorage-independence signifies malignant transformation. Cell–substrate interaction has been shown to impact cell function and modulate cellular sensitivity to extrinsic signals such as growth factor and mechanical stimulation [13,14]. In the current

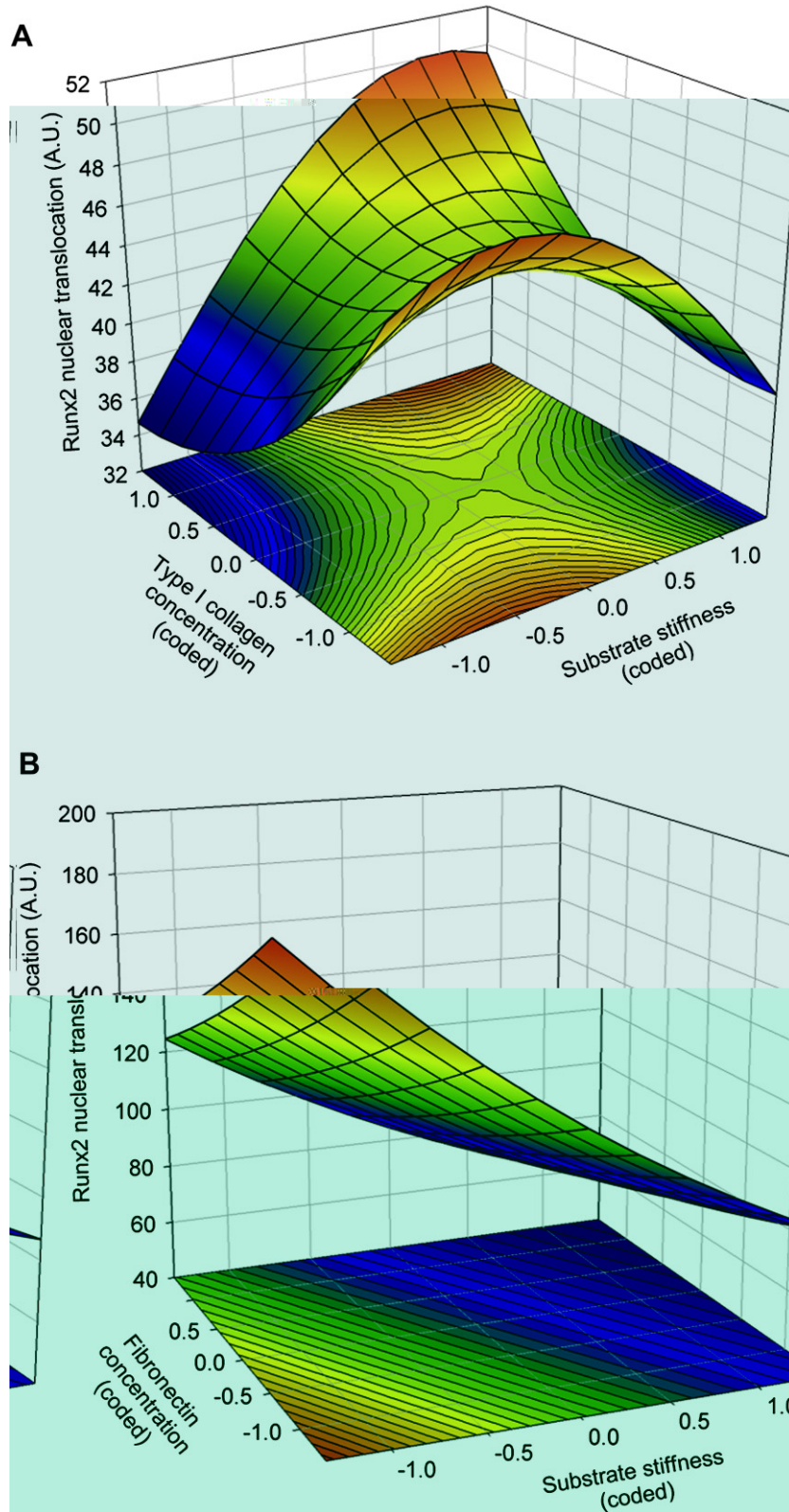


**Fig. 5.** The response surface of MSC osteogenic differentiation on (A) type I collagen- or (B) fibronectin-coated PA substrates. The response map for the collagen-coated substrate based on the full model and illustrates the trend of MSC response, although the model parameters were not statistically significant. The definition of the coded values is provided in Table 1.

study, we investigated the combined effect of matrix elasticity and adhesiveness on MSC spreading, proliferation and osteogenic commitment by incorporating statistical experimental design and analysis with automated high-content microscopy to analyze

thousands of single cells. We efficiently generated response surfaces to facilitate the visualization of how different combinations of matrix stimuli (stiffness and ligand concentration) affect MSC function. The quantification of factor effects and their

presentation in the form of a mathematical function are more descriptive and amenable to optimization than simple pairwise comparisons that are commonly employed. While correlative, empirical modeling can be used to identify phenomena of interest for subsequent mechanistic investigations.

Since ECM-derived signals are transmitted via adhesion-mediated processes, we investigated how MSC spreading was influenced by ECM mechanics and adhesiveness. As expected, increasing substrate stiffness enhanced MSC spreading on both collagen and fibronectin-coated substrates (Fig. 3). Generally, MSC spreading appeared to be highly dependent on substrate mechanics but was insensitive to ECM protein concentrations. Similar observations have been reported for smooth muscle cell spreading on PA substrates, where cell area became independent of protein coating density by 12 h post-seeding [15]. MSC matrix remodeling and deposition of serum-derived proteins might have masked the protein concentration effects. Also, it is important to note that although cell spreading area was positively correlated with substrate rigidities at early time points, morphological differences between the different conditions were negligible (by observation) by day three, possibly due to matrix remodelling as well as contribution from cell–cell contact. Despite the similarity in cell morphology, however, distinct ECM–protein-modulated substrate stiffness influences on MSC proliferation and differentiation were observed, suggesting that ECM–protein-specific substrate mechanics effects were modulated by molecular signalling events that cannot be accounted for by changes in cell shape and/or cytoskeleton tension alone.

In general, MSC functions were more mechanoresponsive on fibronectin than on collagen-coated substrates, as indicated by the greater extent of stiffness-induced changes in MSC response (Figs. 4 and 5). This phenomenon may be attributable to the molecular structure of fibronectin. Fibronectin is a multimodular protein, and cell generated traction forces can induce assembly and unfolding of fibronectin fibrils to expose cryptic binding domains for different integrin interactions [16–18], thereby allowing more degrees of freedom for modulation. The stretching and straightening of fibronectin fibrils could also increase the effective stiffness of the ECM [17,19], eliciting an earlier saturation response at a lower stiffness level. Indeed, both MSC spreading and proliferation on fibronectin-coated substrates exhibited a saturating trend (indicated by a negative quadratic stiffness term,  $\beta_{\text{stiffness}} \cdot \text{stiffness}$ ), whereas on collagen-coated substrates, no saturation was observed within the elastic range studied. It is unclear what caused the observed growth delay on higher stiffness fibronectin-coated substrates. It is unlikely that the cell growth on the highest stiffness fibronectin-coated substrates was contact inhibited, as the total number of cells (estimated by quantifying total DNA) was highest on the intermediate, not highest stiffness substrates (data not shown). A similar reduction in proliferation rate, though less prominent, was reported for a clonally-derived murine stem cell line (D1) on RGD-coated alginate gels, where growth rate was highest on 20 kPa substrates (the lowest stiffness investigated) and lowest on 110 kPa substrates [20]. It is important to note that although our empirical model predicts a maximum proliferation rate (corresponding to 42% BrdU incorporation) on fibronectin-coated substrates with elastic modulus of  $\sim 10$  kPa, doubling the modulus to  $\sim 20$  kPa yielded  $\sim 39\%$  BrdU incorporation. This negligible functional difference suggests that there is a window of tolerance in which changes in material properties do not significantly impact biological function. The identification of such a region permits material optimization for other objectives, such as improving mechanical stability without impacting bioactivity.

The ability to direct differentiation is key to stem cell engineering and generation of replacement tissues. We investigated

how substrate mechanics and surface adhesivity impact early MSC osteogenic commitment. On collagen-coated substrates, there was an interaction between collagen concentration and substrate stiffness. At the lowest collagen concentration ( $7 \mu\text{g/mL}$ , which corresponds to a theoretical density of  $1 \mu\text{g/cm}^2$ ), MSC osteogenic specification revealed a biphasic dependence on substrate stiffness with an optimum at 28.4 kPa, matching previously published results with collagen coating density of  $0.25\text{--}1 \mu\text{g/cm}^2$  [6]. At high collagen concentration ( $\sim 520 \mu\text{g/mL}$  or  $70 \mu\text{g/cm}^2$ ), maximum osteogenic commitment was predicted to be at the higher end of the stiffness scale. Osteogenic differentiation of a pre-osteoblastic cell line (MC3T3-E1) was also shown to increase with increasing substrate stiffness when cultured on poly(ethylene glycol) (PEG) hydrogels functionalized with  $50 \mu\text{g/cm}^2$  of Type I collagen [21]. While these trends were clear and consistent with independent experiments, the model effects were not statistically significant (Fig. 2A), perhaps due to short culture duration and the absence of soluble osteogenic supplements. On fibronectin-coated substrates, Runx2 activation was down-regulated at increasing fibronectin concentration and increasing substrate rigidity. The dominant antagonistic effect of fibronectin-coated substrate stiffness on osteogenic differentiation is consistent with down-regulation of osteocalcin secretion and matrix mineralization by MC3T3-E1 pre-osteoblasts with increasing substrate stiffness (20–110 kPa) on RGD-conjugated alginate gels [22]. In contrast, cytoskeletal tension was positively correlated with osteogenic differentiation on fibronectin in other systems [7,23], suggesting cell-type-specific responses or dependency on other unidentified factors.

The integration of statistical design and analysis of experiments with automated microscopy to study cell–biomaterial interactions is of course not limited to the factors studied here, but is generalizable to combinations of multiple extracellular factors, including other physical and ECM-derived cues and soluble signals. In fact, the power of this approach would be most evident when studying more than two stimuli, as determining higher-order interactions among multiple microenvironmental cues is intractable using OFAT experimental approaches, and requires the efficiency and quantitative nature of the approach used here. Further, the emergence of automated imaging tools with the capabilities of gathering large amount of high-resolution data (both spatial and temporal) of different phenotypic measures reflects the growing push towards a “systems biology” approach that is in line with multifactorial experimentation.

## 5. Conclusion

The integration of rigorous statistical modeling and efficient automated high-content fluorescent microscopy facilitates systematic study of cell–material interactions with practical relevance to the development of biomaterials and engineered tissues. Application of this method demonstrated that MSC function is differentially modulated by substrate mechanics in an ECM-specific manner, suggesting complex interplay between matrix mechanics and biochemistry in the regulation of MSC function.

## Acknowledgements

We acknowledge financial support from the Natural Sciences and Engineering Research Council of Canada and Canadian Institute of Health Research (CHRPJ 323533-06), the Bone and Mineral Scholarship to WLKC, and the Canada Research Chair in Mechanobiology to CAS. We thank William Stanford and Peter Zandstra for access to the Cellomics machines, Paul Cassar and Emanuel Nazareth for technical help with the Cellomics system, and Christopher Moraes for helpful advice.

## Appendix. Supplementary data

Supplementary data associated with this article can be found in the online version, at doi:10.1016/j.biomaterials.2009.12.002.

## References

- [1] Discher DE, Mooney DJ, Zandstra PW. Growth factors, matrices, and forces combine and control stem cells. *Science* 2009;324(5935):1673–7.
- [2] Rehfeldt F, Engler AJ, Eckhardt A, Ahmed F, Discher DE. Cell responses to the mechanochemical microenvironment—Implications for regenerative medicine and drug delivery. *Adv Drug Deliv Rev* 2007;59(13):1329–39.
- [3] Krieg T, LeRoy EC. Diseases of the extracellular matrix. *J Mol Med* 1998;76(3–4):224–5.
- [4] Salaszyk RM, Klees RF, Williams WA, Boskey A, Plopper GE. Focal adhesion kinase signaling pathways regulate the osteogenic differentiation of human mesenchymal stem cells. *Exp Cell Res* 2007;313(1):22–37.
- [5] Klees RF, Salaszyk RM, Kingsley K, Williams WA, Boskey A, Plopper GE. Laminin-5 induces osteogenic gene expression in human mesenchymal stem cells through an ERK-dependent pathway. *Mol Biol Cell* 2005;16(2):881–90.
- [6] Engler AJ, Sen S, Sweeney HL, Discher DE. Matrix elasticity directs stem cell lineage specification. *Cell* 2006;126(4):677–89.
- [7] Rowlands AS, George PA, Cooper-White JJ. Directing osteogenic and myogenic differentiation of MSCs: interplay of stiffness and adhesive ligand presentation. *Am J Physiol, Cell Physiol* 2008;295(4):C1037–44.
- [8] Winer JP, Janmey PA, McCormick ME, Funaki M. Bone marrow-derived human mesenchymal stem cells become quiescent on soft substrates but remain responsive to chemical or mechanical stimuli. *Tissue Eng Part A* 2009;15(1):147–54.
- [9] Pelham Jr RJ, Wang Y. Cell locomotion and focal adhesions are regulated by substrate flexibility. *Proc Natl Acad Sci U S A* 1997;94(25):13661–5.
- [10] Khatiwala CB, Peyton SR, Putnam AJ. Intrinsic mechanical properties of the extracellular matrix affect the behavior of pre-osteoblastic MC3T3-E1 cells. *Am J Physiol, Cell Physiol* 2006;290(6):C1640–50.
- [11] Nakashima K, de Crombrughe B. Transcriptional mechanisms in osteoblast differentiation and bone formation. *Trends Genet* 2003;19(8):458–66.
- [12] Montgomery DC. Design and analysis of experiments. 6th ed. John Wiley & Sons, Inc.; 2005.
- [13] Yip CY, Chen JH, Simmons CA. Engineering substrate mechanics to regulate cell response. In: Khademhosseini A, editor. *Micro- and nanoengineering of the cell microenvironment: technologies and applications*. Boston: London: Artech House; 2008. p. 161–78.
- [14] Kong HJ, Mooney DJ. Microenvironmental regulation of biomacromolecular therapies. *Nat Rev Drug Discov* 2007;6(6):455–63.
- [15] Engler A, Bacakova L, Newman C, Hategan A, Griffin M, Discher D. Substrate compliance versus ligand density in cell on gel responses. *Biophys J* 2004;86(1 Pt 1):617–28.
- [16] Bao G. Protein mechanics: a new frontier in biomechanics. *Exp Mechanics* 2009;49(1):153–64.
- [17] Vogel V, Sheetz MP. Cell fate regulation by coupling mechanical cycles to biochemical signaling pathways. *Curr Opin Cell Biol* 2009;21(1):38–46.
- [18] Hocking DC, Sottile J, Langenbach KJ. Stimulation of integrin-mediated cell contractility by fibronectin polymerization. *J Biol Chem* 2000;275(14):10673–82.
- [19] Antia M, Baneyx G, Kubow KE, Vogel V. Fibronectin in aging extracellular matrix fibrils is progressively unfolded by cells and elicits an enhanced rigidity response. *Faraday Discuss* 2008;139:229–49. discussion 309–25, 419–20.
- [20] Hsiong SX, Carampin P, Kong HJ, Lee KY, Mooney DJ. Differentiation stage alters matrix control of stem cells. *J Biomed Mater Res A* 2008;85(1):145–56.
- [21] Khatiwala CB, Kim PD, Peyton SR, Putnam AJ. ECM compliance regulates osteogenesis by influencing MAPK signaling downstream of RhoA and ROCK. *J Bone Miner Res* 2009;24(5):886–98.
- [22] Kong HJ, Polte TR, Alsberg E, Mooney DJ. FRET measurements of cell-traction forces and nano-scale clustering of adhesion ligands varied by substrate stiffness. *Proc Natl Acad Sci U S A* 2005;102(12):4300–5.
- [23] McBeath R, Pirone DM, Nelson CM, Bhadriraju K, Chen CS. Cell shape, cytoskeletal tension, and RhoA regulate stem cell lineage commitment. *Dev Cell* 2004;6(4):483–95.